Chemical Data Collections 29 (2020) 100530

Contents lists available at ScienceDirect

Chemical Data Collections

journal homepage: www.elsevier.com/locate/cdc

Data Article

Quantum chemical insight into molecular structure, spectroscopic (FT–IR, FT–Raman, UV-vis, NMR), and molecular docking of 3,5-di-tert-butyl-2-hydroxybenzaldehyde

S.J. Jenepha Mary, C. James[†,*]

Department of Physics and Research Centre, Scott Christian College (Autonomous), Nagercoil- 629003, Tamil Nadu, India (Affiliated to Manonmaniam Sundarnar University, Abishekapatti, Tirunelveli 627012, India)

ARTICLE INFO

Article history:
Received 1 May 2020
Revised 23 June 2020
Accepted 27 August 2020
Available online 29 August 2020

Keywords:
NBO
Chemical shift
FT-IR
Raman
Influenza virus

ABSTRACT

The molecule of therapeutic interest 3,5-Di-tert-butyl-2-hydroxybenzaldehyde, a salicylaldehyde derivative has been subjected to FT-IR, FT- Raman, UV-Visible and NMR spectral studies, along with quantum chemical computations using density functional theory. The title molecule has been optimized at B3LYP level of theory and 6-311G+(d,p) basis set. NBO analysis has been performed to study donor acceptor interactions and stability of the molecule arising from hyperconjugative interactions. Spectral analysis has been carried out and the vibrational assignments have been made on potential energy difference. To explain bioactivity several molecular electronic parameters such as frontier molecular orbitals, ESP, charge analysis have been discussed. Antiviral activity of 3,5-Di-tert-butyl-2-hydroxybenzaldehyde has been carried out against influenza viral proteins of type A, type B, type C, and type D. Molecular docking simulations shows it has a good binding affinity toward influenza type D virus.

Specifications Table

Subject area	Spectroscopy and Computational Chemistry
Compound	3,5-Di-tert-butyl-2-hydroxybenzaldehyde
Data category	Computational simulations, Natural bond orbital analysis, vibrational analysis, NMR chemical shift and molecular docking.
Data acquisition format	FT-IR, FT-Raman, NMR, UV-Vis
Data type	Experimental and theoretical
Procedure	Experimental: Sample has been purchased from sigma Aldrich. FT-IR spectrum has been recorded using Perkin-Elmer FT-IR spectrophotometer, FT Raman spectrum has been recorded using BRUKER RFS 27, UV-visible spectrum has been measured using JASCO (V-570) UV/VIS/NIR spectrometer. Computations: Geometry optimization and NBO analysis have been carried out using Gaussian 09 program package and visualized using Gauss view 5.0,Vibrational analysis using MOLVIB 7.0 and molecular docking simulation using AutoDock 4.2 and PYMOL.
Data accessibility	Data is available within the article

* Corresponding author.
E-mail addresses: jenephaashok@gmail.com (S.J. Jenepha Mary), cjamesha@gmail.com (C. James).
† Register number: 18113162132001

https://doi.org/10.1016/j.cdc.2020.100530
2405-8300/

1. Rationale

The outbreak of infections caused by viruses has become a global threat that can result in periodic epidemics, causing high morbidity and mortality in human beings. The development of new antimicrobial agents with low human toxicity is important for the health care system. In search of molecules of therapeutic importance, the molecule 3,5- Di-tert-butyl-2-hydroxybenzaldehyde(TBHB) has been chosen. The present study focuses on the molecular structure, electronic properties, spectral analysis and molecular docking of the title molecule with the hope, the present study may be decisive in the prediction of its mechanism of biological activity.

Hydroxybenzaldehyde derivatives have been found to occur naturally in the plant Gastrodia elata Blume [1]. Benzaldehyde and its hydroxyl derivatives are of significant interest owing to their activity against fungi, cancer, virus, and, bacterial infections [2]. The radical-scavenging and anti-inflammatory activity of hydroxybenzaldehyde in the synthesis of the potent analgesic thiazolo[3,2-b]- [1,2,4] triazole-6(5H)-one has been reported [2,3]. The oxidative property of 4-Hydroxybenzaldehyde is tremendous as it decreases fat accumulation in adipose tissues by activating the fat oxidation and increases leptin signaling [4]. Hydroxybenzaldehydes cause intracellular coagulation of cytoplasmic constituents which leads to cell death or inhibition of cell growth [5,6]. The vibrational modes of the methoxy group and the methyl group of anisaldehyde have been reported [7]. Vibrational spectral studies on flucytosine [8], UV, FT-IR and Raman spectral studies of N,N-dimethyl-3-phenyl-3-pyridin-2-yl-propan-1-amine has been carried out and the spectral bands have been studied [9]. The vibrational bands of the hydroxyl group and aldehyde group in 3-hydroxybenzaldehyde and its cation have been clearly explained [10]. Literature review reveals, the crystal structure of 3,5- Di-tert-butyl-2-hydroxybenzaldehyde [11] has been reported and no other studies on the title molecule have been reported so far. The present work focuses on the structural elucidation of 3,5- Di-tert-butyl-2-hydroxybenzaldehyde and spectral investigation have been carried out using B3LYP /6-31+G (d, p) method. The isotropic chemical shifts computed by ^{13}C and ^{1}H NMR analysis show a good agreement with experimental observations. The molecular electrostatic potential (MEP) surface map shows the reactive sites prone to nucleophilic and electrophilic attack. UV-vis spectrum of the title compound has been calculated and the electronic transition (λmax) has been compared with the experimental value. The Mulliken atomic charges, HOMO, LUMO orbital energy have been analyzed. The presence of the hydrogen bonded intramolecular interactions and the second order perturbation energies due to hyperconjugative interactions have been exposed in NBO analysis. The binding affinity of the ligand protein interactions has been estimated by molecular docking simulation.

2. Procedure

FT IR spectrum has been recorded on a Perkin-Elmer FT-IR spectrophotometer with KBr discs in the range 450-4000 cm-1with a resolution of 1.0 cm-1. FT Raman spectrum has been recorded using BRUKER RFS 27 FT-Raman Spectrometer in the range from 50 to 4000 cm-1 with a resolution of 2 cm-1. The UV-visible absorption spectrum of solid material has been measured in JASCO (V-570) UV/VIS/NIR spectrometer. NMR spectra were recorded using R32 Perkin Elmer NMR spectrometer with DMSO as an internal standard. All the theoretical calculations were carried out using Gaussian 09 software package [12] at the Becke–Lee–Yang–Parr hybrid exchange correlation three parameter functional (B3LYP) level with standard 6-311G(d,p) basis set to derive the optimized geometry. The second order interaction energies between the filled and the vacant orbitals have been carried out using NBO 3.1 program [13] as implemented in the Gaussian 09W package. Normal coordinate analysis (NCA) has been performed to obtain the complete description of the molecular motion using the MOLVIB program version 7.0 written by Sundius [14,15]. 1H and 13C NMR isotropic shielding has been calculated by GIAO method [16,17] and compare with experimental spectra. Auto Dock 4.26 software package has been employed to study the protein-ligand interactions [18] and the binding sites of the protein-ligand have been visualized using PYMOL software [19].

3. Data value and validation

3.1. Structural analysis

The molecular structure of TBHB has been visualized as a benzene ring with an aldehyde group in the 1-position, the hydroxyl group in the ortho position, and a pair of tertiary butyl group in the meta position. The optimized molecular structure of 3,5-di-tertbutyl-2-hydroxy-benzaldehyde has been represented in Fig. 1. Calculated bond lengths and bond angles in comparison with XRD data [11] has been listed in Table S1.

The substitution of the electron donating butyl moiety at 3,5 position and the hydroxyl group at 2-position results in the asymmetry of the phenyl ring as revealed by the bond angles C1-C2-C3 (119.99°), C2-C3-C4(116.38°), C3-C4-C6 (125.34°), C4-C6-C7(116.59°), C1-C7-C6 (121.16°) and C2-C1-C7(120.53°). Also, the bond length C1-C2 and C2-C3 has been increased significantly due to the hydroxyl substituent in the phenyl ring. Calculated dihedral angles C7-C1-C9-O10(-179.98°) and C7-C1-C2-O12(-179.10°) shows that the oxygen atom is coplanar concerning the phenyl ring. The presence of C-H···O intramolecular hydrogen bonded interactions have been observed at H25···O12 (2.346Å) and H22···O12 (2.245Å) which is well within the van der Walls separation between the O atom and H atom. The substitution of the hydroxyl group in TBHB accounts for the antiviral activity [20].

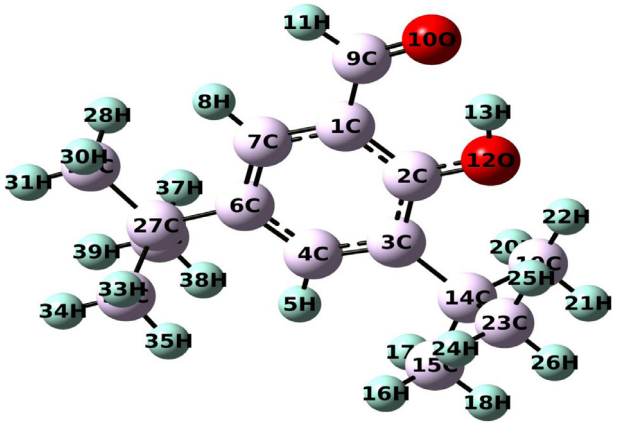

Fig. 1. Optimized structure of TBHB.

Table 1
Second Order Perturbation Theory Analysis of Fock Matrix of TBHB in NBO basis

Donor(i)	ED(i) (e)	Acceptor(j)	ED(j) (e)	E(2) kcal/mol	E(j)−E(i) a.u	F(i,j) a.u
σ (C1-C2)	1.9943	σ*(C1-C7)	0.0201	3.68	1.27	0.061
σ (C1-C2)	1.9943	σ*(C2-C3)	0.0305	3.35	1.24	0.058
σ (C1-C7)	1.9721	σ*(C7-C9)	0.0459	1.95	1.17	0.043
σ (C1-C9)	1.9837	σ*(C6-C7)	0.0208	2.17	1.3	0.047
σ (C2-C3)	1.9729	σ*(C3-C14)	0.0366	2.03	1.09	0.042
σ (C2-C3)	1.9729	σ*(C4-H5)	0.0157	2.09	1.17	0.046
σ (C2-O12)	1.9939	σ*(C3-C4)	0.0187	1.36	1.52	0.041
σ (C3-C4)	1.9723	σ*(C2-O12)	0.0189	3.34	1.08	0.058
σ (C3-C14)	1.9655	σ*(C4-C6)	0.0222	2.7	1.16	0.05
σ (C3-C14)	1.9655	σ*(C14-C19	0.0216	2.66	0.97	0.023
σ (C4-H5)	1.9777	σ*(C2-C3)	0.0305	4.28	1.06	0.06
σ (C4-C6)	1.973	σ*(C3-C14)	0.0366	3.12	1.08	0.052
σ (C6-C7)	1.9751	σ*(C7-C8)	0.0163	1.73	1.17	0.04
σ (C9-O12)	1.9815	σ*(C1-C7)	0.0201	1.48	1.62	0.044
σ (C14-C15)	1.9796	σ*(C14-C23)	0.0216	0.77	0.98	0.024
σ (14-C23)	1.9699	σ*(C3-C14)	0.0366	0.97	0.97	0.024
σ (C27-C32)	1.9714	σ*(C6-C9)	0.0208	1.56	1.13	0.038
n2(O_{12})		π^* (C_1– C_2)	0.44293	37.74	0.33	0.106
		σ *(C_{19}-H_{22})	0.00926	0.51	0.8	0.019
		σ *(C_{23}-H_{25})	0.00926	0.51	0.8	0.019
n1(O_{12})		σ*(C_1-C_2)	0.03461	6.95	1.1	0.078
		σ*(C_{19}-H_{22})	0.00926	1.06	1.06	0.03
		σ*(C_{23}-H_{25})	0.00926	1.06	1.06	0.03

3.2. Natural bond orbital analysis

NBO analysis has been carried out using NBO 3.1 to study the hybridization, hydrogen bonding as well as hyper conjugative interactions that takes place within the Lewis structure of orbitals. The intramolecular hyper conjugative interactions that arise due to the delocalization of electrons are given by the second order perturbation theory. The second order perturbation energy can be calculated using the following relation [21]

$$\Delta E_{ij}^{(2)} = 2\frac{(|(\varphi i|F|\varphi j)|_2}{(\epsilon_i - \epsilon_j)}$$

The strong intra-molecular hyper conjugative interactions are given by the second order perturbation theory analysis is presented in Table 1.

Hyperconjugative interactions from the lone pair oxygen of the hydroxyl group to the antibonding orbitals are n1(O12) → σ*(C1-C2) and n2(O12) → π*(C1-C2) with the stabilization energy of 37.74 kcal/mol and 6.95 kcal/mol respectively. The presence of intramolecular interactions have been observed by the charge transfer that takes place from the lone pair of electrons of the hydroxyl moiety to the antibonding orbitals of the t-butyl moiety, n2(O12) → σ*(C19-H22), n2(O12) → σ*(C23-H25), n1(O12) →σ*(C19-H22) and n1(O12) →σ*(C19-H22) with the stabilization energy of 0.51,0.51, 1.06 and 1.06 kcal/mol.

Table 2
Vibrational assignments of TBHB using normal coordinate analysis based on SQMFF calculations

υ_{IR}	υ_{Raman}	υ_{Scaled}	Assignment with PED (≥10%)
3287w		3287	υOH (100)
3139s	3126w	3136	υRCH (98)
	3053m	3043	$\upsilon_{OPS}CH_3$ (68), $\upsilon_{IPS}CH_3$ (22)
3033m		3040	$\upsilon_{OPS}CH_3$ (67), $\upsilon CH_3$1S(22)
	2994m	2989	υCH_3OS(91)
	2975s	2986	υCH_3OS(99)
1652vvs	1647vvs	1648	CH_3SD(95)
	1598vs	1594	υCHR (69)
	1541w	1548	βRCH (24)
	1393s	1389	υRCC (19)
1382s		1382	υRCC (23)
1363vvs		1358	CH_{3ROCK}(28)
1324vvs	1325vs	1339	$CH_{3ROCK'}$ (25), CH_3ROCK (23),υDCC (16),υRCC(15)
1250	1250w	1269	υRCC (40)
	1221m	1233	ωGCH (56)
1219w		1219	ωGCH (42)
1132w	1130m	1137	ωGCH (43),CHW (41)
1025vvs		1037	RCM (31)
930vvs		930	WGCO (36), PυCK(33),WGCC (18)
	928w	921	RCM(24)
826vvs		823	CCOD (29)
798vs		785	υDCC (55)
	735w	733	τOH (93)
	576m	588	RCM (22)
551m		551	CSD (34)
	534w	529	CSD (19)
	515m	510	ωCO (27)
	413m	423	CR (27)
	288w	288	τCH3 (34)
	268w	266	τCH3 (23)
	116m	116	ATO (30), τCC (19), CRO (13), GCC (12), τCO (10)
	67m	63	τCC (59)

vs- very strong; w-weak; s-strong; υ-stretching; υ_{ss}- symmetric stretching; υ_{AS}-assymmetric stretching; υ_{SD} -Symmetric deformation; υ_{OS}– oυt-plane stretching; υ_{IS} - in-plane stretching; β- in –plane bending; τ-torsion; ω-wagging; G-gaυche; R-Ring; PK- pυckering.

3.3. Vibrational spectral analysis

Vibrational analysis based on both calculated and experimental approach is an efficient tool for the assessment of structural changes and for predicting spectral features. The non-redundant set of internal coordinates has been constructed based on Pulay's recommendations and the assignments of vibrational modes have been made on potential energy distribution (PED) as in Table 2. The observed and simulated FT-IR and FT-Raman spectra of TBHB have been represented in Fig. 2 and Fig. 3 respectively.

3.3.1. Methyl vibrations

Symmetric and asymmetric stretching modes of a methyl group attached to the benzene ring are usually downshifted due to electronic effects resulting from hyper conjugation or back donation of the methyl group with the aromatic ring system. This causes the change in the dipole moment, resulting in the IR spectrum. The asymmetric and symmetric stretching modes of methyl group are expected to be in the region of 2962 cm^{-1} and 2872 cm^{-1} respectively [22,23]. The asymmetric stretching mode is observed as a medium intense band in IR at 3033 cm^{-1}, 3053cm^{-1}, 2994cm^{-1}, and as a strong band in Raman at 2975 cm^{-1}. The symmetric stretching mode is observed at 2910 cm^{-1} in Raman. The out-of-plane bending mode of the methyl group is expected near 1460 cm^{-1}. In TBHB out-of-plane bending mode coupled with CH3 in-plane bending mode has been observed as a strong band at 1445 cm^{-1} in the IR spectrum. C-H out- of- plane and in-plane deformation modes of CH3 group are usually observed at 1450-1450cm^{-1} and 1383-1377cm^{-1} respectively. In TBHB, C-H out-of-plane bending mode has been observed at 1437cm^{-1}, and in-plane bending deformation mode has been observed at 1363cm^{-1}.

3.3.2. Ring vibrations

C-H stretching vibrations of aromatic and heteroaromatic ring cover in the region from 3100 cm^{-1} to 3000 cm^{-1} [22]. The band observed at 3120, 3100, and 3028 cm^{-1} in the FT-IR spectrum and the bands observed at 3125, 3105 cm^{-1} in the Raman spectrum have been assigned to C-H stretching vibrations in the aromatic ring system. C-H bending vibration appears at two distinct regions 1300-1000 cm^{-1} and 700-610 cm^{-1}. The bands at 1200, 1095, and 953 cm-1 in FT-IR and the

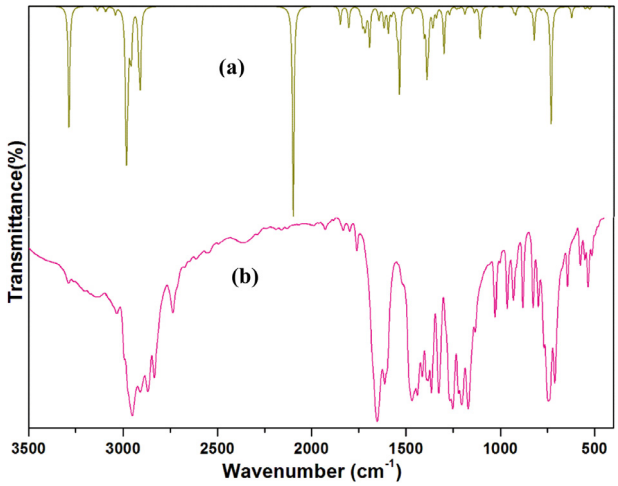

Fig. 2. FT-IR spectra of TBHB (a) Experimental (b) Theoretical.

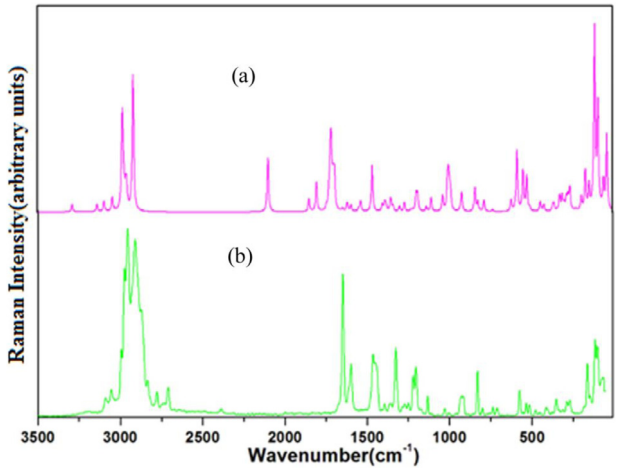

Fig. 3. FT-Raman spectra of TBHB (a) Experimental (b) Theoretical.

bands at 1205, 1090, and 950 cm-^{1} in the FT-Raman spectrum have been assigned to C-H bending vibrations. C-C stretching vibrations in aromatic compounds appear in the region of 1430-1650 cm-^{1} [24]. In TBHB, the prominent peaks at 1652, 1554, 1552, 1509 cm-^{1} in FT-IR, and at 1558, 1508 cm-^{1} in FT-Raman are due to strong C-C stretching. Theoretical values are also in good agreement with the experimental values with the PED contribution of 60 - 77 %. C-C deformation vibration is expected to be in the region 734 cm-^{1} which has been observed in the FT-IR spectrum at 739 cm-^{1}.

3.3.3. Hydroxybenzaldehyde vibrations

In OH, the stretching band generally found in the region 3500cm-^{1} which is likely to be sensitive to the environment, they show pronounced shifts in the spectra of the hydrogen-bonded species. With stronger intermolecular bonding, the O-H stretching vibrations may give rise to broad and intense bands which are often overlaid with peaks due to Fermi-resonance interactions. In TBHB, the band observed at 3218 cm-^{1} in FTIR has been assigned to O-H stretching. The red shift in frequency is due to the hydrogen bonded interactions and this accounts for the biological activity of the molecule. In general, O-H in-plane bending vibration for phenols lies in the region 1150–1250 cm-^{1} and is not much affected due to hydrogen bonding [25]. In HB, the scaled value has been assigned to O-H in-plane bending at 1165 cm-^{1}. The wavenumber increases with hydrogen bond strength because of the large amount of energy required to twist the O-H bond. The C-O-H out-of-plane bending vibration has been noticed in the FT-IR band at 740 cm-1 which is in good agreement with the scaled value (747cm-1). C-O stretching appears as a strong band in the region 1200 cm-^{1} [26]. The C-O stretching vibrations have been observed as a strong band in IR at 1270 cm-^{1} and in Raman at 1275 cm-^{1}.

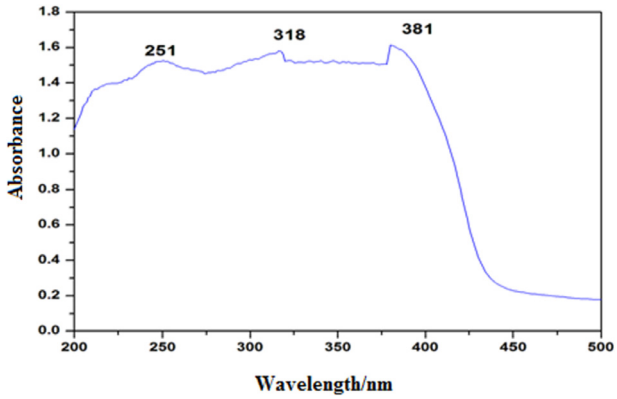

Fig. 4. UV-vis absorption spectrum of TBHB.

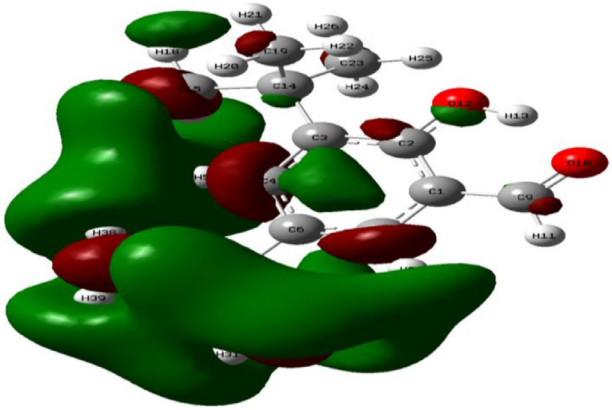

Fig. 5. HOMO Plot of TBHB.

Table 3
HOMO and LUMO energy values of TBHB

Parameters	Values
E_{total} (Hartress)	-153298
E_{HOMO} (au)	-5.3196
E_{LUMO} (au)	-8.5438
$E_{HOMO-LUMO}$ Gap(au)	3.2243
E_{HOMO-1} (au)	-0.3432
E_{LUMO+1} (au)	-0.1396
$E_{HOMO-1\ -\ LUMO+1}$ Gap(au)	0.2037
E_{HOMO-2} (au)	-0.3556
E_{LUMO+2} (au)	-0.1075
$E_{HOMO-2\ -\ LUMO+2}$ Gap (au)	0.2482
Electro negativity χ(au)	-1.6121
Chemical hardness η (au)	-6.9317
Softness ζ(au)	-0.0721
Electrophillicityindex ψ (au)	0.1875

3.4. Analysis of UV spectrum

UV-Vis absorption spectrum of TBHB and 3D plot of HOMO and LUMO have been presented in Fig. 4, Fig. 5 and Fig. 6 respectively. In LUMO, the distributions of charges have been concentrated over the 2-hydroxy benzaldehyde moiety whereas, in LUMO, the distributions of charges have been concentrated over the butyl group. HOMO to LUMO transition implies that electron density transfer takes place from 2-hydroxy benzaldehyde to 3,5 di-tert butyl group. The energy values of HOMO and LUMO and the values of the electronic properties have been given in Table 3. The calculated HOMO and LUMO energies are found to be -5.31955639 eV, and - 8.54383506 eV respectively. The HOMO-LUMO energy gap is calculated to be 3.2242 eV and this small frontier orbital energy gap is more polarized and hence it has high chemical reactivity [27]. HOMO-LUMO

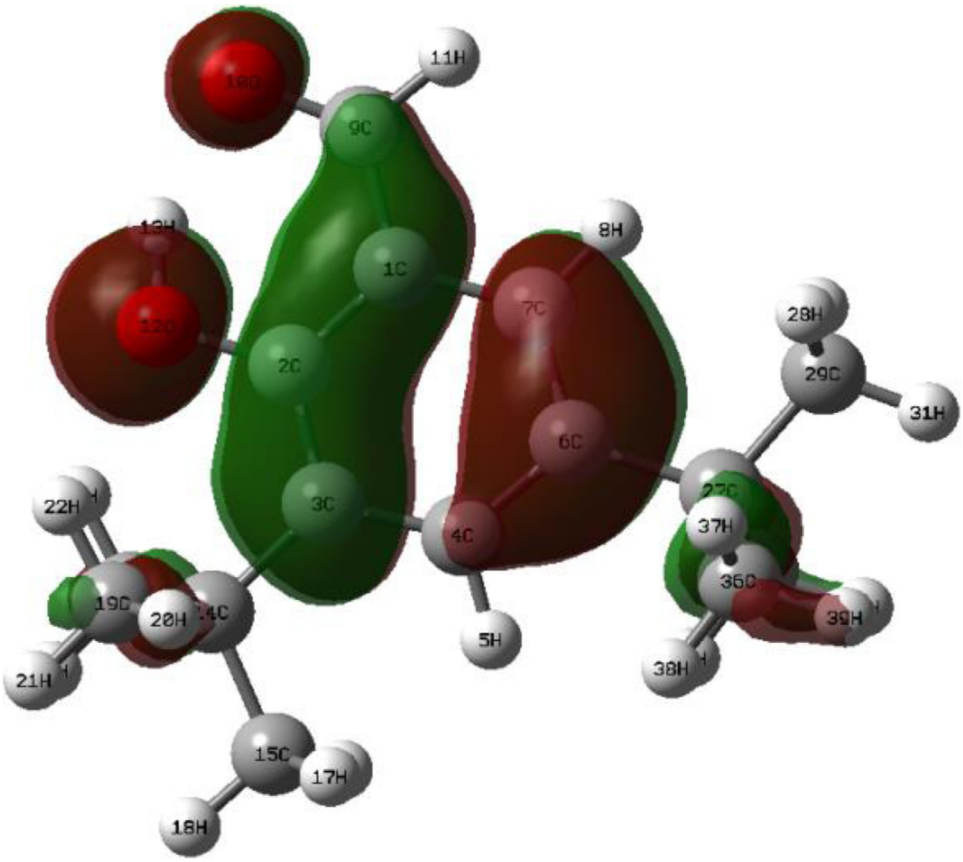

Fig. 6. LUMO Plot of TBHB.

Table 4
UV–vis excitation energy and oscillator strength of TBHB

No.	Energy (cm-1)	Exp.(nm)	Wavelength (nm)	Osc. strength	Symmetry	Major contributions
1	30233	-	330	0.0744	Singlet-A	HOMO→LUMO (96%)
2	32234	318	310	0.0001	Singlet-A	H-2→LUMO (97%)
3	39968	251	250	0.162	Singlet-A	H-1→LUMO (87%)
4	46514	-	214	0.1779	Singlet-A	HOMO→L+1 (65%), HOMO→L+2 (16%)
5	47223	-	211	0.0001	Singlet-A	H-4→LUMO (21%), H-3 →LUMO (74%)
6	49041	-	203	0	Singlet-A	H-4→LUMO (73%), H-3→LUMO (23%)

energy gap is referred to as σ - σ^* transition. The difference in energy ΔE for this electronic transition is 74 kcal/mol. Biochemists and molecular biologists often determine the concentration of a DNA sample for double-stranded DNA at its λmax and maximal absorbance at 260 nm. In TBHB maximal absorbance at 251 nm provides a good indication of the two strands of DNA that can bind to each other. Electronegativity, Chemical hardness, Electrophilicity index are -1.612139335, -6.93169572, -0.072132421, and 0.187471676 respectively (Table 4). Hardness indicates the resistance to the distortion of the electron cloud of chemical systems under small perturbation met during the chemical process.

For electronic transitions of TBHB, TD-DFT calculations have been performed and compared with experimental data as given in Table 4. Visible absorption maxima of TBHB from calculated absorption maxima are 330 nm, 310 nm, 250 nm, 214 nm, 211 nm, and 203 nm. HOMO and LUMO orbitals contributions with their corresponding wavelength show the chemical reactivity. The UV absorption band of benzene is expected to be around 256 nm [28]. In TBHB, the peak has been observed at 251 nm in the experimental spectrum and the corresponding calculated peak has been found at 250 nm, corresponds to the H-1→LUMO (87%) electronic transitions which have been assigned to p→p* transition. Calculated absorption spectra of wavelength 310 nm correspond to the electronic transition from H-2→LUMO with a 96% contribution. Broadening of the UV–Vis absorption spectrum clearly shows the presence of charge transfer interactions.

Table 5
Calculated ^{13}C and ^{1}H NMR spectral values of TBHB in comparison with experimental spectra

Atomic number	Theoretical value	Experimental value	Atomic number	Theoretical value	Experimental value
C1	124.20	120.55	H5	8.83	9.95
C2	165.20	158.30	H8	8.26	9.95
C3	141.80	136.94	H11	10.73	11.69
C4	138.95	131.65	H13	14.05	11.69
C6	144.43	141.89	H16	2.43	2.51
C7	132.89	128.98	H17	2.43	2.50
C9	198.41	199.47	H18	2.03	2.50
C14	47.73	40.38	H20	1.76	1.36
C15	39.16	39.29	H21	1.87	1.28
C19	35.42	35.00	H22	3.43	3.52
C23	35.42	35.00	H24	1.76	1.36

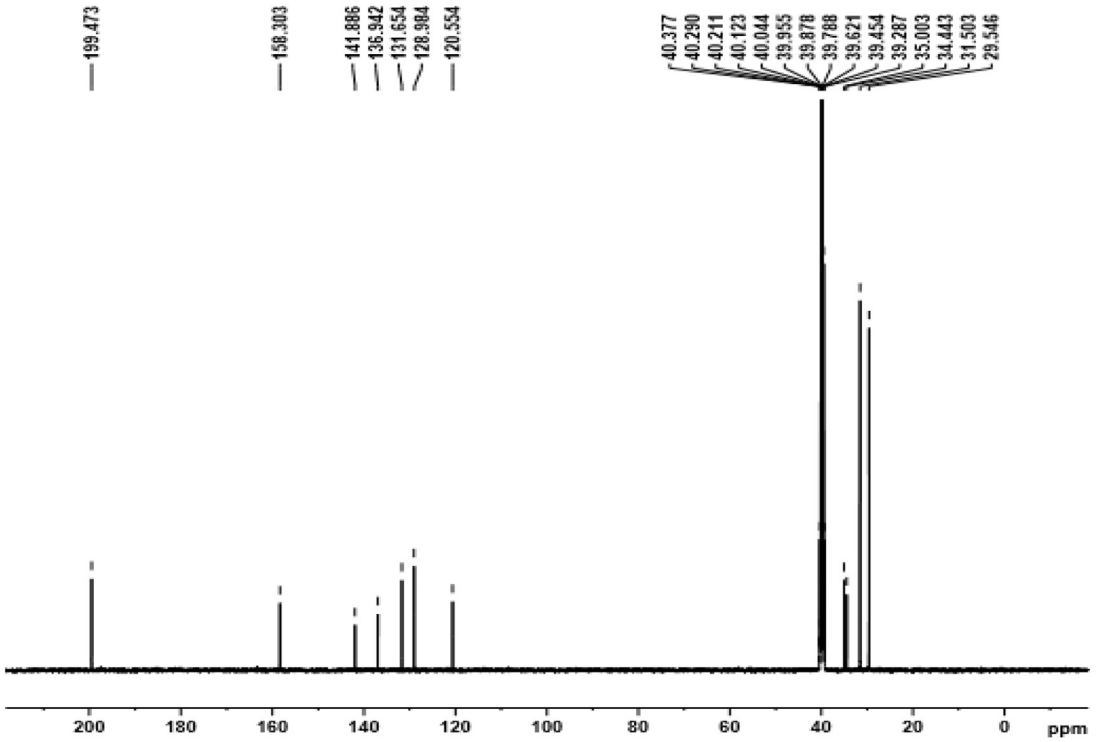

Fig. 7. ^{13}C NMR spectrum of TBHB.

3.5. NMR chemical shifts

Experimental and theoretical values for ^{13}C and ^{1}H NMR spectral chemical shifts have been given in Table 5 and their corresponding spectra have been depicted in Fig. 7 and Fig. 8. All carbon and proton peaks are observed in ^{13}C NMR and ^{1}H NMR with different intensities.^{13}CNMR chemical shifts for organic molecules are observed in the ranges from δ150ppm to δ100ppm [29,30]. C9 and C2 signals appear at δ199.4ppm and δ158.3ppm respectively in the de-shielded region where the chemical shift is higher than the expected region. Here C9 atom is double bonded with oxygen atom only whereas the C2 atom is bonded with an oxygen atom and hydrogen atom. This leads to an increase in the chemical shift on the carbon atom to which the oxygen and hydrogen are attached. This increase in chemical shift is caused by the strong magnetic field due to the removal of electron density and magnetic induction in the neighboring atoms of hydrogen and oxygen.

In the aromatic ring system, the 1HNMR spectrum exhibits proton signals which range from δ8 to δ8.5 ppm. In TBHB these signals have been observed on H5 and H8 (Table 5). But the H11 and H13 have been de-shielded, as they are surrounded by the electronegative oxygen atom resulting in the lowering of electron density around the Hproton and more deshielding the proton experiences.

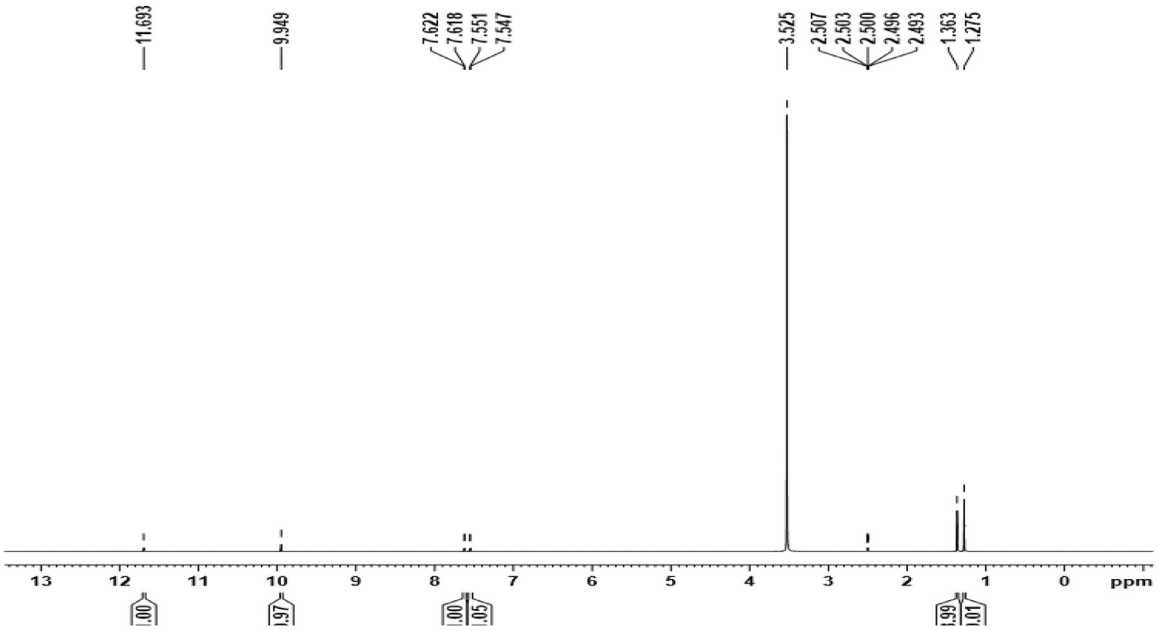

Fig. 8. ^{1}HNMR spectrum of TBHB.

Table 6
Atomic net charges of TBHB

Atomic number	Natural charge	Atomic number	Natural charge
C_1	-0.2440	H_{21}	0.2308
C_2	-0.4071	H_{22}	0.2547
C_3	-0.0706	C_{23}	-0.6809
C_4	-0.1752	H_{24}	0.2320
H_5	0.2376	H_{25}	0.2547
C_6	-0.0543	H_{26}	0.2308
C_7	-0.1840	C_{27}	-0.0617
H_8	0.2386	H_{28}	0.2362
C_9	0.3841	C_{29}	-0.6893
O_{10}	-0.5888	H_{30}	0.2362
H_{11}	0.1692	H_{31}	0.2422
O_{12}	-0.7000	C_{32}	-0.6761
H_{13}	0.5218	H_{33}	0.2393
C_{14}	-0.0622	H_{34}	0.2347
C_{15}	-0.6900	H_{35}	0.2332
H_{16}	0.2340	C_{36}	-0.6761
H_{17}	0.2340	H_{37}	0.2393
H_{18}	0.2440	H_{38}	0.2332
C_{19}	-0.6809	H_{39}	0.2347
H_{20}	0.23203		

3.6. Charge analysis

The atomic natural charges have been calculated for the TBHB molecule and the results have been tabulated in Table 6. It has been observed that positive charges have been concentrated on the hydrogen atoms and negative charges on the carbon atoms with few exceptions. The charge noticed on the C9 atom is found to be positive due to the attachment of the electronegative oxygen atom while other carbon atoms are negative.

The electrostatic potential surface (ESP) of TBHB is shown in Fig. 9. ESP has been found to be a very useful tool to correlate molecular structures and their physiochemical properties in bio-molecules and drugs. In TBHB the interaction of lone pair of electrons with the antibonding provides stabilization to the molecule enhances its bioactivity. The red color region around the oxygen atom of the aldehyde group shows it is most electronegative and the blue color shows the least electronegative region. The red region is the site prone to nucleophilic attack and the blue region is prone to electrophilic attack. These results give information about the region from where the compound can have intra-molecular interaction. This electronegativity oxygen acts as the most reactive part of the molecule.

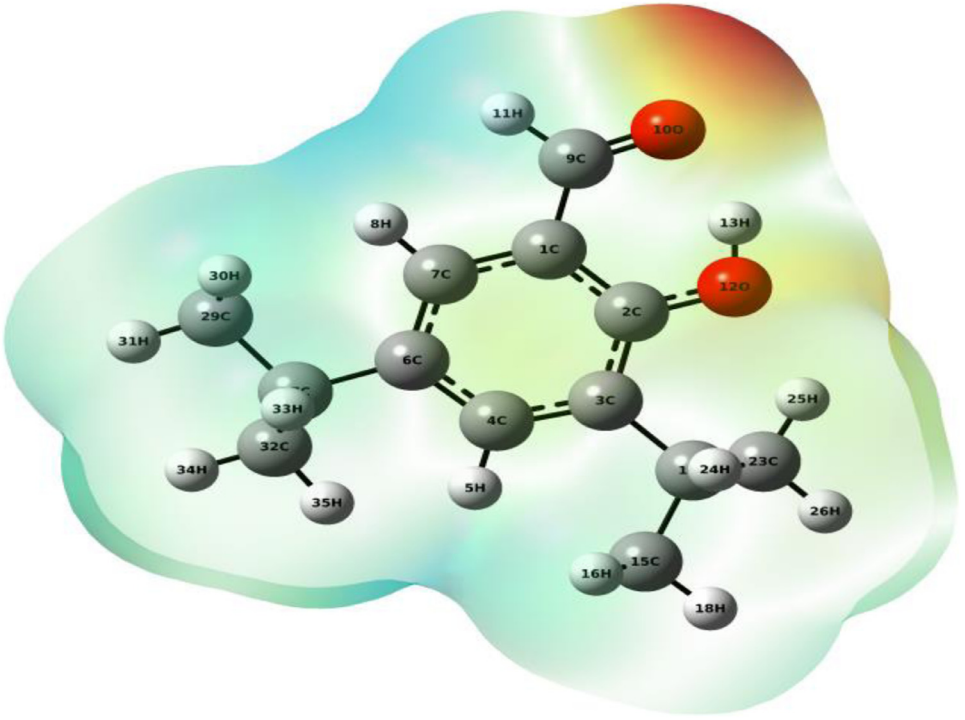

Fig. 9. Electrostatic potential surface of TBHB.

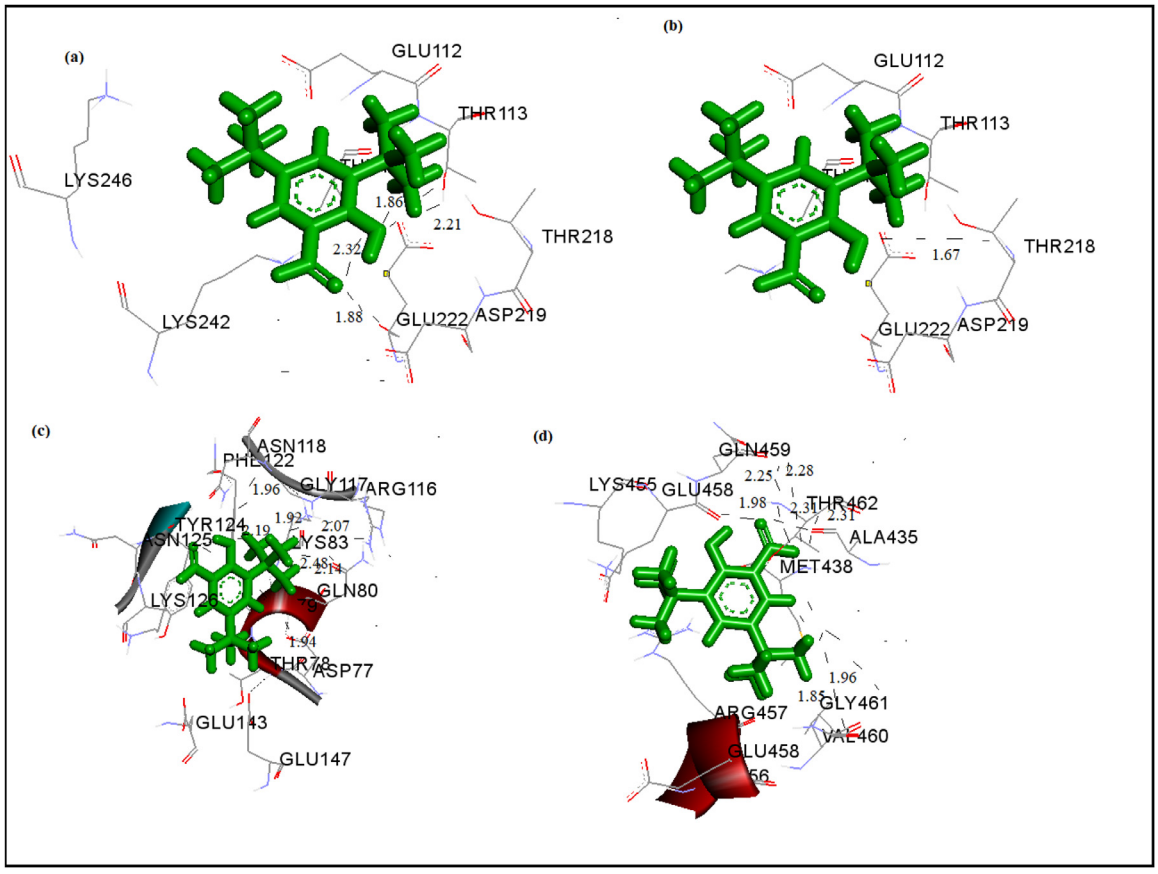

Fig. 10. Pictorial representation of influenza viral proteins after dock (a) Interaction of TBHB with influenza type A protein (b) Interaction of TBHB with influenza type B protein (c) Interaction of TBHB with influenza type c protein (d) Interaction of TBHB with influenza type D protein.

Table 7
Binding free energy and bond distance of TBHB with influenza viral proteins.

Molecule	Protein ID	Binding group	Binding atom	Residues	Bond distance	Binding free energy ΔG(kcal.mol-1)
		Carbonyl		GLU112	1.88	-
TBHB	2v0j		Oxygen	THR113	2.32	7.82
		Hydroxyl		THR113	1.86	
				THR113	2.21	
	3bt6	Hydroxyl	Oxygen	THR218	1.67	-
		Carbonyl		THR78	1.94	7.53
			Oxygen	GLN80	2.14	
	3cw4			LYS83	1.92	-
				LYS83	2.19	8.02
		Hydroxyl		LYS83	2.48	
				LYS83	2.07	
				ASN118	1.96	
		Carbonyl		ALA435	2.31	-
				GLU458	1.98	8.32
				GLN459	2.28	
	5n2u			GLN459	2.25	
		Hydroxyl	Oxygen	THR462	2.31	
				VAL460	1.96	
				GLY461	1.85	

3.7. Molecular docking

Molecular docking of the title molecule has been performed using AutoDock Tools-1.5.4 interfaced with the MGL Tools-1.5.4 package [31]. The antiviral target proteins of the influenza virus of typeA, typeB, typeC and typeD (PDB ID: 2v0j, 3bt6, 3cw4, 5n2u), have been selected for the present docking analysis [32–34] and has been represented in Fig. 10. The three-dimensional (3D) coordinates of the protein file were downloaded from the Research Collaboratory for Structural Bioinformatics (RCSB) protein data bank [35]. The protein preparation has been carried out by the following steps (i) all water molecules were removed (ii) hydrogen atoms were added to the crystal structure (iii) add Coulomb charges (iv) and previously docked inhibitor was removed from the protein. The AutoGrid4.2 [36–37] was used to create affinity grids centred on the active site with 126 * 126* 126 grid size with a spacing of 0.42 Å. The rigid protein and flexible ligand dockings were performed by using AutoDock 4.2 with the Lamarckian genetic algorithm applying the following protocol: trials of 100 dockings, energy evaluations of 25,000,000, the population size of 200, a mutation rate of 0.02, a cross over rate of 0.8, and an elitism value of 1. The protein-ligand interaction complex is given in Fig. 10 and tabulated in Table 7.

The docking results were evaluated by sorting the binding free energy predicted by docking conformations. The predicted best confirmation binding energy have been calculated to be -7.82, -7.53, -8.02, -8.32 kcal/mol which shows the title molecule has pronounced activity against the influenza typeD virus.

4. Conclusion

Structural, vibrational, and electronic properties of 3,5-Di-tert-butyl-2-hydroxybenzaldehyde has been elucidated using experimental techniques (FT-IR, FT-Raman, UV-Vis absorption spectra and NMR) and theoretical studies using density functional theory. NBO reveals the presence of strong hyperconjugative interactions from n1(O12) $\rightarrow \sigma^*$(C1-C2) and n2(O12) $\rightarrow \pi^*$(C1-C2) with the stabilization energy of 37.74 kcal/mol and 6.95 kcal/mol respectively. Vibrational modes have been assigned based on potential energy distribution (PED) and are found to be in good agreement with the experimental data. HOMO-LUMO analysis has been performed to determine the charge transfer within the molecule. UV-vis absorption spectrum reveals the intense band observed at 251 nm provides a good indication that the two strands of DNA is able to bind to each other. Theoretical 1H chemical shifts values have been reported and compared with experimental data which show a very good agreement. Molecular docking simulation of TBHB on influenza viral proteins shows it has a good activity against influenza typeD virus.

Declaration of Competing Interest

None.

References

[1] I Ullah, AL Khan, L Ali2, et al., J. Microbiol. 53 (2015) 127–133.
[2] M.D Mullican, M.W Wilson, D.T Conner, C.K Kostlan, D.J Schrier, Dyer, Med. Chem. 36 (1993) 1090–1099.
[3] S. Fujisawa, Y. Kadoma, I. Yokoe, Chem. Phys. Lipids 130 (2004) 189–195.
[4] S. Park, D.S. Kim, S. Kang, Eur. J. Nutr. 50 (2011) 107–118.
[5] E.R Kenawy, S.D Worley, R. Broughton, Biomacromolecules 8 (2007) 1359–1384.

[6] E.S Park, W.S Moon, M.J Song, M.N Kim, K.H Chung, J.S Yoon, Int. Biodeter. Biodegr. 47 (2001) 209–214.
[7] S. Gunasekaran, S. Seshadri, S. Muthu, S. Kumaresan, R. Arunbalaji, Spectrochim. Acta Part A 70 (2008) 550–556.
[8] S. Renuga, M. Karthikesan, S. Muthu, Spectrochim. Acta Part A 127 (2014) 439–453.
[9] S. Seshadri, S. Gunasekaran, S. Muthu, S. Kumaresan, R. Arunbalaji, J. Raman Spectrosc. 38 (2007) 1523–1531.
[10] S. Muthu, M. Prasath, Spectrochim. Acta Part A 115 (2013) 789–799.
[11] DM. Tooke, AL. Spek, Acta Crystallogr. Sect. E. 60 (2004) 0766–0767.
[12] M.J. Frisch, G.W. TrucksGaussian 09, Revision B.01, Gaussian 09, Gaussian, Inc., Wallingford CT, 2009.
[13] E.D Glendening, A.E Reed, J.E Carpenter, F. Weinhold, NBO Version 3.1, TCI University of Wisconsin, Madison, 1998.
[14] T. Sundius, J. Mol. Struct. 218 (1990) 321.
[15] T. Sundius, Vib. Spectrosc. 29 (2002) 89.
[16] R. Duchfield, J. Chem. Phys. 56 (1972) 5688.
[17] K. Wolinski, J.F. Hinton, P. Pulay, J. Am. Chem. Soc. 112 (1990) 8251.
[18] G.M. Morris, D.S. Goodsell, R.S. Halliday, R. Huey, W.E. Hart, R.K. Belew, A.J. Olson, J. Comput. Chem. 19 (1998) 1639–1662.
[19] The PyMOL Molecular Graphics System, LLC, Schrodinger, 2009 Version 1.
[20] G.B. Tolstorozhev, et al., J. Appl. Spectrosc. 79 (2012) 658.
[21] A.E. Reed, L.A. Curtiss, F. Weinhold, Chem. Rev. 88 (1988) 899.
[22] G. Varsanyi, Assignments for Vibrational Spectra of Seven Hundred Benzene Derivatives, 1e2, Adam Hilger, London, 1974.
[23] R.M. Silverstein, F.X. Webster, Spectrometric Identification of Organic Compounds, John Wiley and Sons, New York, 2003.
[24] N.B. Colthup, L.H. Daly, S.E. Wiberley, Introduction to Infrared and Raman Spectroscopy, Academic Press, New York, 1990.
[25] B.C. Smith, Infrared Spectral Interpretation, CRC Press, Boca Raton, FL, 1996.
[26] G. Gece, Corros. Sci. 50 (2011) 2981–2992.
[27] J. Mohan, "Organic Analytical Chemistry Theory and Practice", Published by Narosa Publication House, New Delhi. Page no. 347-350.
[28] H.O. Kalinowski, S. Berger, S. Braun, Carbon-13 NMR Spectroscopy, John Wiley & Sons, Chichester, 1988.
[29] K. Pihlaja, E. Kleinpeter (Eds.), Carbon-13 Chemical Shifts in Structural and Stereochemical Analysis, VCH Publishers, Deerfield Beach, 199
[30] G.M Morris, R. Huey, W. Lindstrom, M.F Sanner, R.K Belew, D.S Goodsell, Olson, J. Comput. Chem. 16 (2009) 2785–2791.
[31] I. Mochalkin, S. Lightle, Y. Zhu, J.F. Ohren, C. Spessard, N.Y. Chirgadze, C. Banotai, M. Melnick, L. McDowell, Protein Sci. 16 (2007) 2657–2666.
[32] Q. Wang, F. Cheng, M. Lu, X. Tian, J. Ma, J. Virol. 82 (2008) 3011–3020.
[33] T. Kuzuhara, D. Kise, H. Yoshida, T. Horita, Y. Murazaki, A. Nishimura, N. Echigo, H. Utsunomiya, H. Tsuge, J. Biol. Chem. 284 (2009) 6855–6860.
[34] A. Donchet, J. Oliva, A. Labaronne, L. Tengo, M. Miloudi, F.C.A. Gerard, C. Mas, G. Schoehn, R.W.H. Ruigrok, M. Ducatez, T. Crépin, Sci. Rep. 9 (2019) 1–9.
[35] F.C. Bernstein, T.F. Koetzle, G.J. Williams, E.E. Meyer Jr., M.D. Brice, J.R. Rodgers, O. Kennard, T. Shimanouchi, Tasumi, J. Mol. Biol. 112 (1977) 535–542.
[36] G.M. Morris, D.S Goodsell, R.S Halliday, R. Huey, W.E Hart, R.K Belew, A.J Olson, J. Comput. Chem. 19 (1998) 1639–1662.
[37] R. Huey, G.M. Morris, A.J. Olson, D.S. Goodsell, J. Comput. Chem. 28 (2007) 1145–1152.